Title
Visualizing heavy fermions emerging in a quantum critical Kondo lattice.

Journal
Nature, 486(7402)

ISSN
0028-0836

Authors
Aynajian, Pegor
da Silva Neto, Eduardo H
Gyenis, András
et al.

Publication Date
2012-06-01

DOI
10.1038/nature11204

ARTICLE

doi:10.1038/nature11204

Visualizing heavy fermions emerging in a quantum critical Kondo lattice

Pegor Aynajian[1]*, Eduardo H. da Silva Neto[1]*, András Gyenis[1], Ryan E. Baumbach[2], J. D. Thompson[2], Zachary Fisk[3], Eric D. Bauer[2] & Ali Yazdani[1]

In solids containing elements with *f* orbitals, the interaction between *f*-electron spins and those of itinerant electrons leads to the development of low-energy fermionic excitations with a heavy effective mass. These excitations are fundamental to the appearance of unconventional superconductivity and non-Fermi-liquid behaviour observed in actinide- and lanthanide-based compounds. Here we use spectroscopic mapping with the scanning tunnelling microscope to detect the emergence of heavy excitations with lowering of temperature in a prototypical family of cerium-based heavy-fermion compounds. We demonstrate the sensitivity of the tunnelling process to the composite nature of these heavy quasiparticles, which arises from quantum entanglement of itinerant conduction and *f* electrons. Scattering and interference of the composite quasiparticles is used to resolve their energy–momentum structure and to extract their mass enhancement, which develops with decreasing temperature. The lifetime of the emergent heavy quasiparticles reveals signatures of enhanced scattering and their spectral lineshape shows evidence of energy–temperature scaling. These findings demonstrate that proximity to a quantum critical point results in critical damping of the emergent heavy excitation of our Kondo lattice system.

A local magnetic moment occurs when a strongly interacting quantum state, such as an atomic *d* or *f* orbital, cannot be doubly occupied owing to strong on-site Coulomb repulsion[1]. In the presence of a dilute concentration of such magnetic moments in a metal, spin-flip scattering of conduction electrons from these local moments results in their collective magnetic screening below a characteristic temperature called the Kondo temperature, T_K (Fig. 1a)[2]. In materials where local moments are arranged in a dense periodic array, the so-called Kondo lattice, the deconfinement of localized orbitals through their hybridization with the conduction electrons results in composite low-energy excitations with a heavy effective mass (Fig. 1b). Tuning the hybridization between *f* orbitals and itinerant electrons can destabilize the heavy Fermi-liquid state towards an antiferromagnetically ordered ground state at a quantum critical point (QCP)[3–8]. In proximity to such a quantum phase transition—between itinerancy and localization of *f* electrons—many heavy-fermion systems exhibit unconventional superconductivity at low temperatures (Fig. 1c)[9].

Thermodynamic and transport studies have long provided evidence for heavy quasiparticles, their unconventional superconductivity and non-Fermi-liquid behaviour in a variety of material systems[9–14]. However, the emergence of a coherent band of heavy quasiparticles near the Fermi energy in a Kondo lattice system is still not well understood[14–17]. Part of the challenge has been the inability of spectroscopic measurements to probe the development of heavy quasiparticles with lowering of temperature and to characterize their properties with high energy resolution. Such precise measurements of heavy-fermion formation are not only required for understanding the nature of these electronic excitations close to quantum phase transitions[18], but are also critical to identifying the source of unconventional superconductivity near such transitions.

Composite heavy-fermion excitations

The emergence of composite heavy fermions in a Kondo lattice can be considered as a result of the hybridization of two electronic bands: one

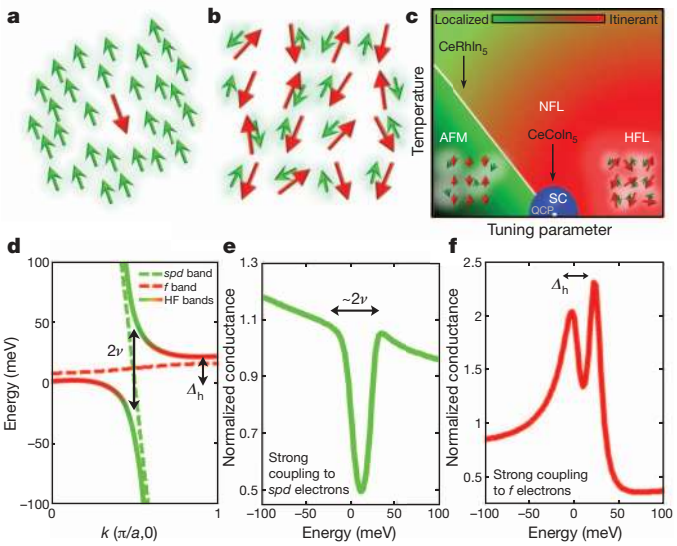

Figure 1 | Tunnelling into a Kondo lattice. **a**, **b**, Schematic representations of a single-impurity Kondo effect (**a**) and a Kondo lattice (**b**), illustrating the screening (hybridization) of the local moments (red arrows) by the itinerant conduction electrons (green arrows). **c**, Schematic phase diagram of heavy-fermion systems where the electronic ground state can be tuned from antiferromagnetism (AFM) with localized *f* moments to a heavy Fermi liquid (HFL) with itinerant *f* electrons. At low temperatures, superconductivity (SC) sets in near the quantum critical point (QCP) from a non-Fermi liquid (NFL). Insets show cartoon pictures of the spin fluctuations in the different phases. **d**, Bare electronic bands (dashed lines; *spd* and *f*) and hybridized heavy-fermion bands (HF; solid lines) displaying a direct (2ν) and an indirect (Δ_h) hybridization gap. **e**, Tunnelling spectrum computed from the hybridized band structure in **d** for a tunnelling ratio $t_f/t_c = -0.025$, showing sensitivity to the direct hybridization gap (2ν). **f**, Similar spectra computed with $t_f/t_c = -0.37$, showing sensitivity to the indirect gap (Δ_h). See Supplementary Information section I for details of the model.

[1]Joseph Henry Laboratories and Department of Physics, Princeton University, Princeton, New Jersey 08544, USA. [2]Los Alamos National Laboratory, Los Alamos, New Mexico 87545, USA. [3]Department of Physics and Astronomy, University of California, Irvine, California 92697, USA.
*These authors contributed equally to this work.

dispersing band due to conduction electrons and one weakly dispersing band originating from localized *f* electrons (dashed lines in Fig. 1d). This hybridization generates low-energy quasiparticles that are a mixture of conduction electrons and *f* electrons with a modified band structure characterized by the so-called direct ($2v$) and indirect (Δ_h) hybridization gaps, as shown in Fig. 1d[17,19]. Various theoretical approaches, including several numerical studies, reproduce the generic composite band structure shown in Fig. 1d[20–24]. Recent theoretical modelling has also shown that tunnelling spectroscopy can be a powerful probe of this composite nature of heavy fermions[25–28]. Depending on the relative tunnelling amplitudes to the light conduction (t_c) or to the heavy *f*-like (t_f) components of the composite quasiparticles, and due to their interference, tunnelling spectroscopy can be sensitive to different features of the hybridized band structure. Figure 1d–f shows examples of model calculations (see Supplementary Information section I) illustrating the sensitivity of the spectra to predominant tunnelling to the light (Fig. 1e) or heavy (Fig. 1f) electronic states.

Recent advances in the application of scanning tunnelling microscopy (STM) to heavy fermions are providing a new approach to examining the correlated electrons in these systems with high energy and spatial resolutions. STM and point-contact experiments on heavy-fermion compounds have shown evidence for hybridization of the conduction electrons with the *f* orbitals and have been used to probe the so-called hidden order phase transition involving heavy *f* electrons in URu_2Si_2 (refs 29–32). Sudden onset of the hidden order phase seems to give rise to strong modification of the band structure in URu_2Si_2 as detected by STM measurements[30,31]. However, these changes are correlated with the phase transition into the hidden order at 17.5 K rather than being the generic physics of heavy Fermi liquids that should appear at higher temperatures and evolve smoothly with lowering of temperature. Direct experimental observation of the gradual formation of heavy quasiparticles with decreasing temperature and evidence of their composite nature, which is ubiquitous to all heavy fermions, as well as examination of their properties in proximity to QCPs, have remained out of the reach of STM and other spectroscopic measurements.

$CeMIn_5$ as a model heavy-fermion system

To provide a controlled study of the emergence of heavy-fermion excitations within a Kondo lattice system that can be tuned close to a QCP, we carried out studies on the $CeMIn_5$ (with M = Co, Rh) material system. These so-called 115 compounds (the chemical formula could be written $Ce_1M_1In_5$) offer the possibility of tuning the interaction between the *f* orbitals of Ce and the itinerant *spd* conduction electrons using isovalent substitutions at the transition metal site within the same tetragonal crystal structure. Consequently, the ground state of this system can be tuned (in stoichiometric compounds) between antiferromagnetism, as in $CeRhIn_5$ (Néel temperature $T_N = 3.5$ K), to superconductivity, as observed in $CeCoIn_5$ (superconducting transition temperature $T_c = 2.3$ K) and $CeIrIn_5$ ($T_c = 0.4$ K)[9]. Previous studies indicate that $CeCoIn_5$ is very close to a QCP[33–36], whereas $CeRhIn_5$ can be tuned close to this transition with application of pressure[7,37]. These experiments confirm that superconductivity in the 115 system emerges at low temperatures close to a QCP from heavy low-energy excitations that developed at high temperature[7,9,36]. More specifically, transport studies show a drop in the electrical resistivity of $CeCoIn_5$ around 50 K (which has been interpreted as evidence for the development of a coherent heavy quasiparticle band) followed by a *T*-linear resistivity at lower temperature (above T_c)[38] — a behaviour that has been associated with the proximity to the QCP. Quantum oscillations and thermodynamic measurements find a heavy electron effective mass (10–50 m_0, where m_0 is the bare electron mass) for $CeCoIn_5$, whereas in the same temperature range the *f* electrons in $CeRhIn_5$ are effectively decoupled from the conduction electrons[39,40].

Figure 2 shows STM images of a single crystal of $CeCoIn_5$ that has been cleaved *in situ* in our variable temperature ultrahigh-vacuum STM. In this family of compounds, the cleaving process results in the exposure of multiple surfaces terminated with different chemical compositions. The crystal symmetry necessarily requires multiple surfaces for cleaved samples, as no two equivalent consecutive layers occur within the unit cell. Therefore breaking of any single chemical bond will result in different layer terminations on the two sides of the cleaved sample. Experiments on many cleaved samples have revealed three different surfaces, two of which are atomically ordered (termed surfaces A and B in Fig. 2a, b) with a periodicity of ~4.6 Å corresponding to the lattice constant of the bulk crystal structure, whereas the third surface (termed surface C, Fig. 2b) is reconstructed. Comparison of the relative heights of the sub-unit-cell steps between the different layers (Fig. 2c, d) to the crystal structure determined from scattering experiments[41] suggests that exposed surfaces A, B and C correspond to the Ce–In, Co and In_2 layers, respectively. Experiments on $CeCo(In_{0.9985}Hg_{0.0015})_5$ and $CeRhIn_5$ reveal similar results, where cleaving exposes the corresponding multiple layers in those compounds (see Supplementary Information section II). Hg defects in $CeCoIn_5$ at this concentration have negligible influence on its thermodynamic and transport properties and are introduced for the scattering experiments described below[42].

Signatures of hybridization and composite excitations

Spectroscopic measurements of $CeCoIn_5$ show the sensitivity of the tunnelling process to the composite nature of the hybridized heavy-fermion states. Tunnelling spectra on surface A (identified as the Ce–In layer) of $CeCo(In_{0.9985}Hg_{0.0015})_5$ show that on cooling the sample dramatic changes develop in the spectra in an asymmetric fashion about the Fermi energy (Fig. 3a). (The same behaviour is also observed in $CeCoIn_5$; see Supplementary Information section III.)

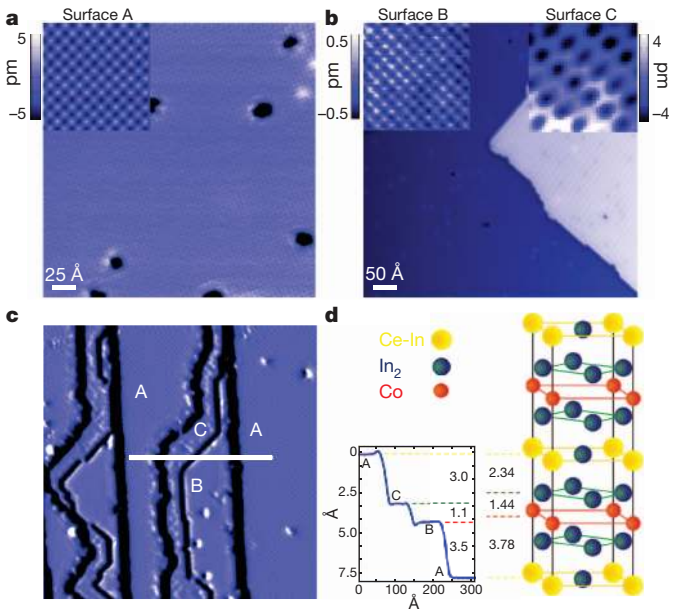

Figure 2 | STM topographies on $CeCoIn_5$. **a**, Constant current topographic image (+200 mV, 200 pA) showing an atomically ordered surface (termed surface A) with a lattice constant of ~4.6 Å. **b**, Topographic image (−200 mV, 200 pA) showing two consecutive layers: a distinct atomically ordered surface (termed surface B, lattice constant ~4.6 Å, dark blue) and a reconstructed surface (termed surface C, light blue). Insets in **a** and **b** show magnified images (45×45 Å^2) of the three different surfaces. **c**, Constant current topographic image (−150 mV, 365 pA) displaying all three surfaces (the derivative of the topography is shown to enhance contrast). **d**, A line section through the different surfaces (solid line in **c**) showing the relative step heights (left) compared to the bulk crystal structure (right).

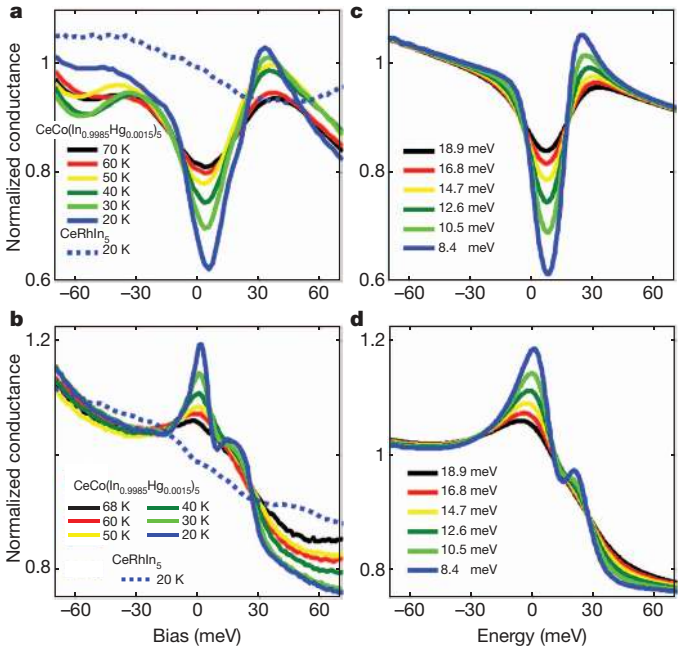

Figure 3 | Composite nature of heavy-fermion excitations. **a** Averaged tunnelling spectra (−150 mV, 200 pA) measured on surface A of $CeCo(In_{0.9985}Hg_{0.0015})_5$ for different temperatures (T, in K; solid lines) and on the corresponding surface A of $CeRhIn_5$ at 20 K (dashed line). **b**, Averaged tunnelling spectra (−150 mV, 200 pA) measured on surface B of $CeCo(In_{0.9985}Hg_{0.0015})_5$ for different temperatures (T, in K; solid lines) and on corresponding surface B of $CeRhIn_5$ at 20 K (dashed line). **c**, **d**, Tunnelling spectra computed for $t_f/t_c = -0.01$ (**c**) and $t_f/t_c = -0.20$ (**d**) for selected values of γ_f (in meV; solid lines). See Supplementary Information section I for details of the model.

The redistribution of the spectra observed on this surface is consistent with a tunnelling process that is dominated by coupling to the light conduction electrons and displays signatures of the direct hybridization gap ($2v$) experienced by this component of the heavy-fermion excitations (for example, see Fig. 1d, e). In contrast to these observations, similar measurements on the corresponding surface of $CeRhIn_5$ show spectra that are featureless in the same temperature range (Fig. 3a, dashed line) and are consistent with the more localized nature of the Ce f orbitals in $CeRhIn_5$ as compared to $CeCoIn_5$. The hybridization gap structure in $CeCoIn_5$ is also centred above the chemical potential (8 meV, see Fig. 3a), which makes access difficult for angle-resolved photoemission experiments[43–45]—the typical technique used for probing electronic band structure in solids.

The composite nature of the heavy-fermion excitations manifests itself by displaying different spectroscopic characteristics for tunnelling into the different atomic layers. Figure 3b shows spectra measured on surface B (identified as Co) of $CeCo(In_{0.9985}Hg_{0.0015})_5$ that look very different from those measured on surface A (Fig. 3a). In the temperature range where spectra on surface A (Fig. 3a) develop a depletion of spectral weight near the Fermi energy, surface B shows a sharp enhancement of spectral weight within the same energy window (Fig. 3b). With further lowering of temperature, the enhanced tunnelling on surface B evolves into a double-peak structure. As a control experiment, measurements on the corresponding surface in $CeRhIn_5$, once again, display no sharp features in the same temperature and energy windows (Fig. 3b, dashed line). The spectroscopic features of surface B of $CeCo(In_{0.9985}Hg_{0.0015})_5$ display the characteristic signatures of dominant tunnelling to the f component of the heavy quasiparticles, which reside near the Fermi energy and are expected to display the indirect hybridization gap (Δ_h; see Fig. 1d, f).

Modelling the tunnelling to composite heavy excitations can reproduce our spectroscopic measurements on the two different atomically ordered surfaces of $CeCo(In_{0.9985}Hg_{0.0015})_5$. Following recent theoretical efforts[26,27], we compute spectroscopic properties of a model band structure in which a single hole-like itinerant band of *spd*-like electrons hybridizes with a narrow band of *f*-like electrons (see Supplementary Information section I for details of the model). The results of our calculations (Fig. 3c, d) are sensitive to the ratio of tunnelling (t_f/t_c) into the heavy f states to tunnelling into the light conduction band—a behaviour that explains the differences between the tunnelling processes on the different cleaved surfaces (Fig. 3a, b). Although naively one would expect that tunnelling to the heavy excitations would be more pronounced on the Ce–In layer, recent first principles calculations show that the amplitude of the hybridization of the f states with the out-of-plane *spd* electrons can be remarkably larger than the amplitude of the hybridization with the in-plane *spd* electrons[21].

Visualizing quasiparticle mass enhancement

To directly probe the energy–momentum structure of heavy quasiparticles in the 115 material systems, we have carried out spectroscopic mapping with the STM that enables us to visualize the scattering and interference of these quasiparticle excitations from impurities or structural defects. Elastic scattering of quasiparticles from these imperfections gives rise to standing waves in the conductance maps at wavelengths corresponding to $2\pi/q$, where $\mathbf{q} = \mathbf{k}_f - \mathbf{k}_i$ is the momentum transfer between initial ($\mathbf{k}_i$) and final ($\mathbf{k}_f$) states at the same energy. We expect that those $\mathbf{q}$ with the strongest intensity connect regions of high density of states on the contours of constant energy, and hence provide energy–momentum information about the quasiparticle excitations. We characterize the scattering $\mathbf{q}$ using discrete Fourier transforms (DFTs) of STM conductance maps measured at different energies. The presence of Hg substitutions in $CeCo(In_{0.9985}Hg_{0.0015})_5$ provides a sufficient number of scattering centres to enhance signal to noise ratio for such quasiparticle interference (QPI) measurements.

Figure 4a shows examples of energy-resolved STM conductance maps on surface A of $CeCo(In_{0.9985}Hg_{0.0015})_5$ measured at 20 K; the maps display signatures of scattering and interference of quasiparticles from defects and step edges. These conductance maps show clear changes of the wavelength of the modulations as a function of energy. Perhaps the most noticeable are the changes around each random defect (see Supplementary Information section II for the corresponding STM image showing the location of the Hg defects). Figure 4b shows DFTs of such maps; sharp non-dispersive Bragg peaks (at the corners, $(\pm 2\pi/a, 0), (0, \pm 2\pi/a)$) corresponding to the atomic lattice are seen, as well as other features (concentric square-like shapes) that rapidly disperse with energy, collapse (Fig. 4b; 0 meV) and then disappear (Fig. 4b; 9 meV) near the Fermi energy. We have carried out such measurements both at low temperatures (20 K, Fig. 4b), where the spectrum shows signatures of hybridization between conduction electrons and f orbitals, and at high temperatures (70 K, Fig. 4c), where such features are considerably weakened (for example, Fig. 4c; 2 meV, 10 meV). As a control experiment, we have also carried out the same measurements on the corresponding surface of $CeRhIn_5$ (Fig. 4d), for which signatures of heavy electron behaviour are absent (for example, Fig. 3a) in the same temperature window (20 K). Although understanding details of the QPI in Fig. 4 requires detailed modelling of the band structure of the 115 compounds, the square-like patterns observed in the data correspond to scattering wavevectors that can be identified from the calculated local-density approximation (LDA) band structure[46] (see Supplementary Information section V).

We find that analysing the features of the energy-resolved DFT maps provides direct evidence for mass enhancement of quasiparticles, in unison with related signatures in the tunnelling spectra. Figure 5a and b shows line sections of the DFT maps plotted along two high-symmetry directions (the thick white lines in Fig. 4b) as a function of energy for $CeCo(In_{0.9985}Hg_{0.0015})_5$ at 20 K, and in Fig. 5c we show their

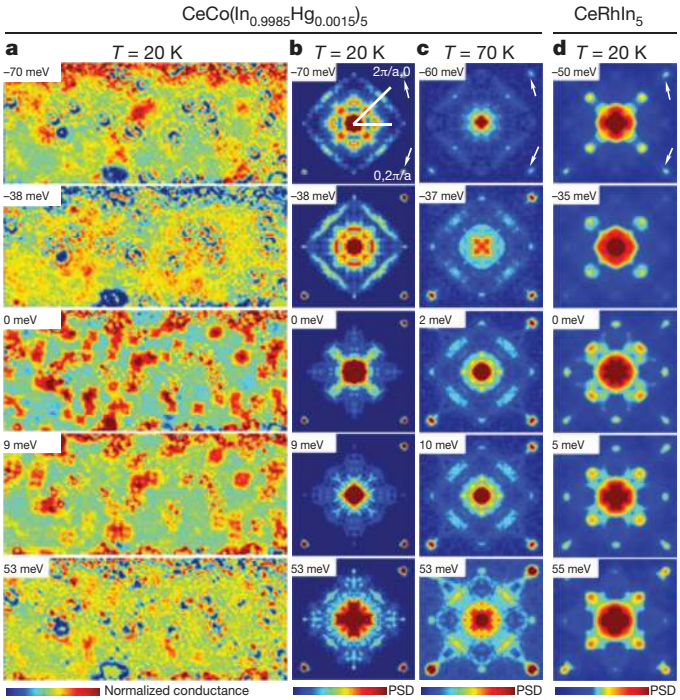

Figure 4 | Spectroscopic mapping of quasiparticle interference (QPI). **a**, **b**, Real space (**a**) and corresponding DFT (**b**) of conductance maps (−200 mV, 1.6 nA) at selected energies (top left of each panel) measured on surface A of $CeCo(In_{0.9985}Hg_{0.0015})_5$ at 20 K. **c**, **d**, Similar DFTs for $CeCo(In_{0.9985}Hg_{0.0015})_5$ at 70 K (−150 mV, 1.5 nA; **c**) and on the corresponding surface A for $CeRhIn_5$ at 20 K (−200 mV, 3.0 nA; **d**) at selected energies. Arrows indicate the position of the Bragg peaks at $(2\pi/a, 0)$ and $(0, 2\pi/a)$. All DFTs were four-fold symmetrized (due to the four-fold crystal symmetry) to enhance resolution (see Supplementary Information section IV). The intensity is represented on a linear scale. PSD, power spectrum density.

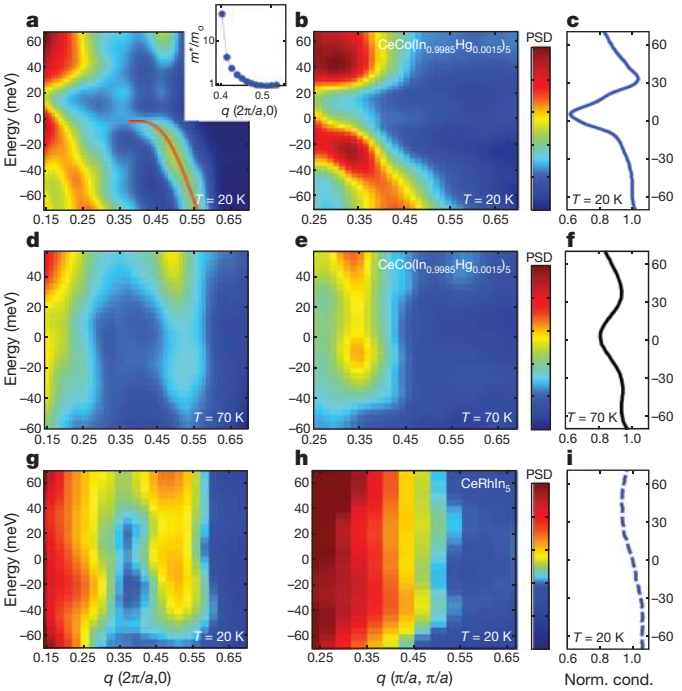

Figure 5 | Visualizing quasiparticle mass enhancement. **a**, **b**, Energy–momentum structure of the QPI bands extracted from line sections (solid white lines in Fig. 4b) along the atomic direction $(2\pi/a, 0)$ (**a**) and along the zone diagonal $(\pi/a, \pi/a)$ (**b**) in $CeCo(In_{0.9985}Hg_{0.0015})_5$ at 20 K. The solid red line represents a fourth-order polynomial fit to the data. Inset in **a** shows the effective mass m^*/m_0 as a function of momenta obtained from the curvature ($\frac{1}{4}\hbar^2 (d^2E/dq^2)^{-1}$) of the outer band (solid red line in **a**). **c**, Average spectrum on surface A of $CeCo(In_{0.9985}Hg_{0.0015})_5$ at 20 K, reflecting the suppression of scattering in the QPI bands. Similar measurements performed in $CeCo(In_{0.9985}Hg_{0.0015})_5$ at 70 K (**d**–**f**) and in $CeRhIn_5$ at 20 K (**g**–**i**). The intensity is represented on a linear scale.

corresponding spatially averaged spectrum. The square-like regions of enhanced quasiparticle scattering in Fig. 4b appear in the line sections of Fig. 5a, b as energy-dependent bands of scattering, which become strongly energy dependent near the Fermi energy. Clearly the scattering of the quasiparticle excitations in the energy window near the direct hybridization gap has a flatter energy–momentum structure than that at energies away from the gap. This is a direct signature of the quasiparticles acquiring heavy effective mass at low energies near the Fermi energy. Detailed analysis of one of the QPI bands estimates the mass enhancement near the Fermi energy to be about $30m_0$ (Fig. 5a inset), a value which is close to that seen in quantum oscillation studies of $CeCoIn_5$ (refs 39, 40). Our model calculation, which describes the spectroscopic lineshapes on the different surfaces, can also be extended to reproduce the signatures of mass enhancement in the QPI data (see Supplementary Information section I).

Contrasting low temperature QPI patterns on $CeCo(In_{0.9985}Hg_{0.0015})_5$ to measurements on the same compound at high temperatures (70 K, Fig. 5d, e), where the hybridization gap is weak (Fig. 5f), or to measurements on $CeRhIn_5$ (20 K, Fig. 5g, h), where signatures of a hybridization gap are absent in the tunnelling spectra (Fig. 5i), confirms that the development of this gap results in apparent splitting of the bands and is responsible for both the scattering and the heavy effective mass in the QPI measurements. Furthermore, these measurements show that the underlying band structure responsible for the scattering wavevectors away from the Fermi energy is relatively similar between $CeCo(In_{0.9985}Hg_{0.0015})_5$ and $CeRhIn_5$. Only when f electrons of the Kondo lattice begin to strongly hybridize with conduction electrons and modify the band structure within a relatively narrow energy window (30 meV) do we see signatures of heavy-fermion excitations in QPI measurements, signalling a transition from a small to a large Fermi surface (see Supplementary Information section V).

Signatures of quantum criticality

The ability to tunnel through the f component of the heavy quasiparticles on surface B of $CeCo(In_{0.9985}Hg_{0.0015})_5$ provides an opportunity to probe the lifetime of the heavy quasiparticles as a function of temperature in a system that is close to a QCP. The narrow dispersion of the f band results in a direct connection between the experimentally measured width of the peak in the density of states near the Fermi energy (Fig. 3b) and the lifetime of the heavy quasiparticles. Analysis of this width measured at different temperatures is displayed in Fig. 6a (see Supplementary Information section VI), and shows a strong temperature dependence with a finite intercept (~3.5 meV) in the limit of zero temperature. The finite width at zero temperature can be understood as a consequence of a small but finite dispersion of the f band as well as a finite probability of tunnelling into the *spd* electrons (see Supplementary Information section I). However, the large linear slope in Fig. 6a (that is, larger than $3/2\ k_BT$, where k_B is Boltzmann's constant and T is temperature) indicates that the lifetime of the f electrons, as opposed to thermal broadening, is strongly influencing the spectra and its temperature dependence. Consistent with this observation, we also find that to capture the temperature evolution of the spectra in Fig. 3b, we have to use rather large values of scattering rate (inverse lifetime) of the f component of the heavy quasiparticles, $\gamma_f = \hbar/\tau_f$ (where $\hbar$ is Planck's constant h divided by 2π and τ_f is the lifetime of the quasiparticles), in our model calculations (Fig. 3d).

A T-linear scattering rate (or inverse lifetime) for the heavy quasiparticles is consistent with the expectation that $CeCoIn_5$ is close to a QCP, because for systems tuned close to such transitions, temperature is the only relevant energy scale available to determine the quasiparticle lifetime, resulting in $\hbar/\tau_f \propto k_BT$ (refs 18, 47). However, a more precise signature of a QCP would be the observation

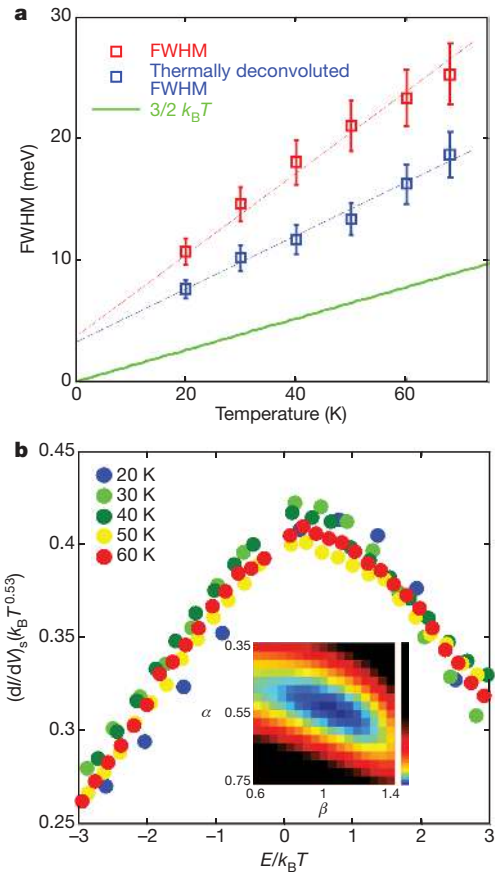

Figure 6 | Signatures of quantum criticality. **a**, Full width at half maximum (FWHM) of the heavy quasiparticle peak (red squares) as a function of temperature extracted from a Gaussian fit to the sharp lineshape of the spectra of Fig. 3b after a smooth background subtraction (see Supplementary Information section VI). Blue squares represent the thermally deconvoluted FWHM corresponding to the intrinsic width in the absence of thermal broadening. The green line represents $3/2k_BT$. Error bars, 1 s.d. **b**, Energy–temperature scaling of the different spectra of Fig. 3b, after the removal of a temperature independent background (see Supplementary Information sections VI and VII), within a narrow energy window near the Fermi energy. Key shows temperature T in K. Inset shows the 'goodness of the collapse' (colour scale) as a function of the critical exponents α and β.

of energy–temperature scaling of experimental quantities near such transitions. In fact, recent theoretical work suggests that the instability of the Fermi surface near a QCP should result in scaling properties of the single-particle excitation that can be directly probed in measurements of the tunnelling density of states[48]. To test this hypothesis, we examine the lineshape of the tunnelling spectra on surface B of $CeCo(In_{0.9985}Hg_{0.0015})_5$ near the chemical potential at different temperatures, and attempt to scale the data (Fig. 3b) by plotting $(dI/dV)_S(k_BT^{\alpha})$ as a function of $E/(k_BT)^{\beta}$. (Here $(dI/dV)_S$ is the background-subtracted spectra of Fig. 3b (see Supplementary Information section VI) and E is the energy of the tunnelling quasiparticles.) We find that using the exponents $\alpha = 0.53$ and $\beta = 1$ results in a collapse of the data at different temperatures on a single curve in the low bias region (see Fig. 6b and Supplementary Information section VII). Although an understanding of the value of the exponent α is currently lacking, the linear power β confirms our hypothesis of energy–temperature scaling associated with proximity to a QCP. These results indicate that the heavy quasiparticles in $CeCoIn_5$ are damped because of critical fluctuations rather than the typical scattering that is expected in a Fermi liquid (T^2 dependence). Similar energy–temperature scalings, with anomalous exponents (α), have been previously observed in the dynamical spin susceptibility of other heavy-fermion systems near QCPs[3,5,49,50]. However, here we show for the first time that the signatures of scaling and critical phenomena appear in the spectroscopic properties of the quasiparticle excitations.

Conclusion and outlook

The experimental results and the model calculations presented here provide a comprehensive picture of how heavy-fermion excitations in the 115 Ce-based Kondo lattice systems emerge with lowering of temperature or as a result of chemical tuning of the interaction between the Ce *f* electrons and the conduction electrons. The changes in the scattering properties of the quasiparticles directly signal the flattening of their energy–momentum structure and the emergence of heavy quasiparticles near the Fermi energy. Such changes are also consistent with the predicted evolution from a small to a large Fermi surface as the localized *f* electrons hybridize with the conduction electrons. The sensitivity of the tunnelling to the surface termination and the successful modelling of these data provide direct spectroscopic evidence of the composite nature of heavy fermions and offer a unique method to disentangle their components.

Our experiments also demonstrate that the emergent heavy quasiparticles in our system are strongly scattered and show signatures of scaling associated with critical damping of excitations in proximity to a QCP. Like many other heavy-fermion systems, thermodynamic and transport studies of the 115 systems have shown evidence of quantum criticality, but such signatures have not been previously isolated in an electron spectroscopy measurement, as described here. Such spectroscopic signatures are direct evidence for the breakdown of coherent fermionic excitations approaching a QCP. Future extension of our measurements to lower temperatures could probe the interplay between quantum fluctuations and the appearance of superconductivity, an issue which continues to be one of the most debated in condensed matter physics.

METHODS SUMMARY

The single crystals of $CeCoIn_5$, $CeCo(In_{0.9985}Hg_{0.0015})_5$ and $CeRhIn_5$ used for this study were grown from excess indium at Los Alamos National Laboratory. Small, flat crystals were oriented along the crystallographic axes and cut into sizes suitable for STM measurements ($\sim 2 \times 2 \times 0.2\ mm^3$). The samples were cleaved on a surface perpendicular to the *c* axis in ultrahigh vacuum (UHV) and transferred *in situ* to the microscope head. Differential conductance (dI/dV) measurements were performed using standard lock-in techniques. Approximately ten different samples of $CeCoIn_5$, $CeCo(In_{0.9985}Hg_{0.0015})_5$ and $CeRhIn_5$ were successfully cleaved and studied, and the spectroscopic data collected were reproducible on the corresponding identical exposed surfaces of the different samples. Spectra measured at different locations on each surface showed negligible variations. The spectra presented here (in the main paper) are averaged over approximately 200 individual spectra measured over an area of at least 100 Å × 100 Å. The spectroscopic lineshapes showed negligible variations as the tip height was varied (variation of the tunnelling current by two orders of magnitude).

Received 21 December 2011; accepted 30 April 2012.

1. Anderson, P. W. Localized magnetic states in metals. *Phys. Rev.* **124,** 41–53 (1961).
2. Shiba, H&. Kuramoto, Y. (eds) Kondo effect — 40 years after the discovery. *J. Phys. Soc. Jpn* **74,** 1–238 (2005).
3. Schroder, A. *et al.* Onset of antiferromagnetism in heavy-fermion metals. *Nature* **407,** 351–355 (2000).
4. Coleman, P., Pépin, C., Si, Q. & Ramazashvili, R. How do Fermi liquids get heavy and die? *J. Phys. Condens. Matter* **13,** 723–738 (2001).
5. Si, Q., Rabello, S., Ingersent, K. & Smith, J. L. Locally critical quantum phase transitions in strongly correlated metals. *Nature* **413,** 804–808 (2001).
6. Senthil, T., Sachdev, S. & Vojta, M. Fractionalized Fermi liquids. *Phys. Rev. Lett.* **90,** 216403 (2003).
7. Park, T. *et al.* Hidden magnetism and quantum criticality in the heavy fermion superconductor $CeRhIn_5$. *Nature* **440,** 65–68 (2006).
8. Gegenwart, P., Si, Q. & Steglich, F. Quantum criticality in heavy-fermion metals. *Nature Phys.* **4,** 186–197 (2008).
9. Pfleiderer, C. Superconducting phases of f-electron compounds. *Rev. Mod. Phys.* **81,** 1551–1624 (2009).
10. Palstra, T. T. M. *et al.* Superconducting and magnetic transitions in the heavy-fermion system URu_2Si_2. *Phys. Rev. Lett.* **55,** 2727–2730 (1985).
11. Stewart, G. Heavy-fermion systems. *Rev. Mod. Phys.* **56,** 755–787 (1984).

12. Fisk, Z., Sarrao, J. L., Smith, J. L. & Thompson, J. D. The physics and chemistry of heavy fermions. *Proc. Natl Acad. Sci. USA* **92,** 6663–6667 (1995).
13. Steglich, F. *et al.* Classification of strongly correlated f-electron systems. *J. Low Temp. Phys.* **99,** 267–281 (1995).
14. Yang, Y.-f., Fisk, Z., Lee, H.-O., Thompson, J. D. & Pines, D. Scaling the Kondo lattice. *Nature* **454,** 611–613 (2008).
15. Si, Q. & Steglich, F. Heavy fermions and quantum phase transitions. *Science* **329,** 1161–1166 (2010).
16. Anderson, P. W. Fermi sea of heavy electrons (a Kondo lattice) is never a Fermi liquid. *Phys. Rev. Lett.* **104,** 176403 (2010).
17. Coleman, P. in *Handbook of Magnetism and Advanced Magnetic Materials* Vol. 1 (eds Kronmeuller, H. & Parkin, S.) 45 (Wiley and Sons, 2007).
18. Sachdev, S. *Quantum Phase Transitions* (Cambridge Univ. Press, 1999).
19. Varma, C. M. Mixed-valence compounds. *Rev. Mod. Phys.* **48,** 219–238 (1976).
20. Grenzebach, C., Anders, F. B., Czycholl, G. & Pruschke, T. Transport properties of heavy-fermion systems. *Phys. Rev. B* **74,** 195119 (2006).
21. Shim, J. H., Haule, K. & Kotliar, G. Modeling the localized-to-itinerant electronic transition in the heavy fermion system $CeIrIn_5$. *Science* **318,** 1615–1617 (2007).
22. Martin, L. C., Bercx, M. & Assaad, F. F. Fermi surface topology of the two-dimensional Kondo lattice model: dynamical cluster approximation approach. *Phys. Rev. B* **82,** 245105 (2010).
23. Jacob, D., Haule, K. & Kotliar, G. Dynamical mean-field theory for molecular electronics: electronic structure and transport properties. *Phys. Rev. B* **82,** 195115 (2010).
24. Benlagra, A., Pruschke, T. & Vojta, M. Finite-temperature spectra and quasiparticle interference in Kondo lattices: from light electrons to coherent heavy quasiparticles. *Phys. Rev. B* **84,** 195141 (2011).
25. Yang, Y.-f. Fano effect in the point contact spectroscopy of heavy-electron materials. *Phys. Rev. B* **79,** 241107 (2009).
26. Maltseva, M., Dzero, M. & Coleman, P. Electron cotunneling into a Kondo lattice. *Phys. Rev. Lett.* **103,** 206402 (2009).
27. Figgins, J. & Morr, D. K. Differential conductance and quantum interference in Kondo systems. *Phys. Rev. Lett.* **104,** 187202 (2010).
28. Wölfle, P., Dubi, Y. & Balatsky, A. V. Tunneling into clean heavy fermion compounds: origin of the Fano line shape. *Phys. Rev. Lett.* **105,** 246401 (2010).
29. Park, W. K., Sarrao, J. L., Thompson, J. D. & Greene, L. H. Andreev reflection in heavy-fermion superconductors and order parameter symmetry in $CeCoIn_5$. *Phys. Rev. Lett.* **100,** 177001 (2008).
30. Aynajian, P. *et al.* Visualizing the formation of the Kondo lattice and the hidden order in URu_2Si_2. *Proc. Natl Acad. Sci. USA* **107,** 10383–10388 (2010).
31. Schmidt, A. R. *et al.* Imaging the Fano lattice to 'hidden order' transition in URu_2Si_2. *Nature* **465,** 570–576 (2010).
32. Ernst, S. *et al.* Emerging local Kondo screening and spatial coherence in the heavy-fermion metal $YbRh_2Si_2$. *Nature* **474,** 362–366 (2011).
33. Sidorov, V. A. *et al.* Superconductivity and quantum criticality in $CeCoIn_5$. *Phys. Rev. Lett.* **89,** 157004 (2002).
34. Paglione, J. *et al.* Field-induced quantum critical point in $CeCoIn_5$. *Phys. Rev. Lett.* **91,** 246405 (2003).
35. Paglione, J., Sayles, T. A., Ho, P. C., Jeffries, J. R. & Maple, M. B. Incoherent non-Fermi-liquid scattering in a Kondo lattice. *Nature Phys.* **3,** 703–706 (2007).
36. Urbano, R. R. *et al.* Interacting antiferromagnetic droplets in quantum critical $CeCoIn_5$. *Phys. Rev. Lett.* **99,** 146402 (2007).
37. Hegger, H. *et al.* Pressure-induced superconductivity in quasi-2D $CeRhIn_5$. *Phys. Rev. Lett.* **84,** 4986–4989 (2000).
38. Petrovic, C. *et al.* Heavy-fermion superconductivity in $CeCoIn_5$ at 2.3 K. *J. Phys. Condens. Matter* **13,** 337–342 (2001).
39. Hall, D. *et al.* Fermi surface of the heavy-fermion superconductor $CeCoIn_5$: the de Haas–van Alphen effect in the normal state. *Phys. Rev. B* **64,** 212508 (2001).
40. Shishido, H., Settai, R., Hashimoto, S., Inada, Y. & Ōnuki, Y. De Hass van Alphen effect of $CeRhIn_5$ and $CeCoIn_5$ under pressure. *J. Magn. Magn. Mater.* **272–276,** 225–226 (2004).
41. Moshopoulou, E. G. *et al.* Comparison of the crystal structure of the heavy-fermion materials $CeCoIn_5$, $CeRhIn_5$ and $CeIrIn_5$. *Appl. Phys. A* **74,** s895–s897 (2002).
42. Booth, C. H. *et al.* Local structure and site occupancy of Cd and Hg substitutions in $CeTIn_5$ (T=Co, Rh, and Ir). *Phys. Rev. B* **79,** 144519 (2009).
43. Fujimori, S. *et al.* Direct observation of a quasiparticle band in $CeIrIn_5$: an angle-resolved photoemission spectroscopy study. *Phys. Rev. B* **73,** 224517 (2006).
44. Ehm, D. *et al.* High-resolution photoemission study on low-T_K Ce systems: Kondo resonance, crystal field structures, and their temperature dependence. *Phys. Rev. B* **76,** 045117 (2007).
45. Koitzsch, A. *et al.* Hybridization effects in $CeCoIn_5$ observed by angle-resolved photoemission. *Phys. Rev. B* **77,** 155128 (2008).
46. Oppeneer, P. M. *et al.* Fermi surface changes due to localized–delocalized f-state transitions in Ce-115 and Pu-115 compounds. *J. Magn. Magn. Mater.* **310,** 1684–1690 (2007).
47. Sachdev, S. & Ye, J. Universal quantum-critical dynamics of two-dimensional antiferromagnets. *Phys. Rev. Lett.* **69,** 2411–2414 (1992).
48. Senthil, T. Critical Fermi surfaces and non-Fermi liquid metals. *Phys. Rev. B* **78,** 035103 (2008).
49. Aronson, M. C. *et al.* Non-Fermi-liquid scaling of the magnetic response in $UCu_{5-x}Pd_x$ (x=1,1.5). *Phys. Rev. Lett.* **75,** 725–728 (1995).
50. Schröder, A., Aeppli, G., Bucher, E., Ramazashvili, R. & Coleman, P. Scaling of magnetic fluctuations near a quantum phase transition. *Phys. Rev. Lett.* **80,** 5623–5626 (1998).

Supplementary Information is linked to the online version of the paper at www.nature.com/nature.

Acknowledgements We acknowledge discussions with P. W. Anderson, E. Abrahams, P. Coleman, N. Curro, D. Pines, D. Morr, T. Senthil, S. Sachdev, M. Vojta, C. Varma and C. V. Parker. Work at Princeton University was primarily supported by a grant from the DOE Office of Basic Energy Sciences (DE-FG02-07ER46419). The instrumentation and infrastructure at the Princeton Nanoscale Microscopy Laboratory are also supported by grants from the NSF-DMR1104612 and NSF-MRSEC programmes through the Princeton Center for Complex Materials (DMR-0819860), and the W.M. Keck foundation as well as the Eric and Linda Schmidt Transformative fund at Princeton. P.A. acknowledges postdoctoral fellowship support through the Princeton Center for Complex Materials funded by the NSF-MRSEC programme. Work at Los Alamos National Laboratory was performed under the auspices of the US Department of Energy, Office of Basic Energy Sciences, Division of Materials Science and Engineering. Z.F. acknowledges support from NSF-DMR-0801253.

Author Contributions P.A., E.H.d.S.N. and A.G. performed the STM measurements. P.A. and E.H.d.S.N. analysed the data. E.H.d.S.N. and P.A. performed the theoretical calculations. R.E.B., J.D.T., Z.F. and E.D.B. synthesized and characterized the materials. A.Y., P.A. and E.H.d.S.N. wrote the manuscript. All authors commented on the manuscript.

Author Information Reprints and permissions information is available at www.nature.com/reprints. The authors declare no competing financial interests. Readers are welcome to comment on the online version of this article at www.nature.com/nature. Correspondence and requests for materials should be addressed to A.Y. (yazdani@princeton.edu).